Dynamical Behavior and Stability Analysis of Hydromechanical Gates

Fabian A. Bernhard¹ and Paolo Perona²

Abstract: This study revisits the stability of hydromechanical gates for upstream water surface regulation, also known as AMIL gates. AMIL gates are used in irrigation canals, where they are often installed in series. From the regulation perspective, instabilities are undesired because they generate waves and fluctuations in the discharge. A mathematical model for an AMIL gate is described as a nonlinear dynamical system, which permits analyzing the dynamic interaction between the local water level and the gate position. The feedback effect of the gate on the water level is introduced by considering a storage volume of length *l*. In the derived model, waves are simplified to fluctuations of the flat water surface of the storage volume. Although previous studies used the same model, none has clarified the sensitivity of the model to the parameter *l*. The role of this parameter is investigated and it is calibrated with experimental measurements. The precision of the regulation is described by the decrement, the range of the water level around the target level. Based on the mathematical model, a relationship for calibration of the gate and precision of regulation is presented. The subsequent stability analysis of the dynamical system focuses on five control parameters and sheds light on their influence on the gate behavior. Hopf bifurcations are identified, which separate stable equilibrium solutions from stable periodic solutions. Further work might consider the implications of the periodic solutions on gates that work in series, as well as envision the innovative use of such gates outside of the domain of irrigation canals to obtain dynamic environmental flows in hydropower systems. **DOI:** 10.1061/(ASCE)IR.1943-4774.0001209. © 2017 American Society of Civil Engineers.

Introduction

Hydromechanical gates for upstream water surface regulation, also known as AMIL gates, are used in gravity irrigation systems to control water levels upstream of their location for varying flow rates in the main canal (Rogers and Goussard 1998; Ramirez-Luna 1997; Montañés 2005; GEC Alsthom 1992). This flow rate may vary if the inflow upstream changes or as water is removed via lateral off-takes from the main canal according to a varying demand.

AMIL gates are a specific type of radial gates, used as automatic control structures in order to cope with these variations in flow rate by opening or closing in response to the current water level. Their objective is to maintain the water level in a certain range around their trunnion axis. This range is referred to as *decrement* (Ramirez-Luna 1997; GEC Alsthom 1992) and can be related to the gate properties (calibration of mass and center of gravity).

A photo and an illustration of an AMIL gate are shown in Figs. 1 and 2. In addition to typical radial gates, they are equipped with a toroidal float attached to the upstream side of the gate leaf, counterweights on the downstream side, and a damping device to reduce oscillations. Because the gate is operated only by the water force, AMIL gates are counted among the hydromechanical gates (Cassan et al. 2011).

Note. This manuscript was submitted on December 21, 2016; approved on March 7, 2017; published online on July 7, 2017. Discussion period open until December 7, 2017; separate discussions must be submitted for individual papers. This paper is part of the *Journal of Irrigation and Drainage Engineering*, © ASCE, ISSN 0733-9437.

Through the interaction of the gate and the local water level, oscillations are possible and are indeed observed, particularly when the damping element is worn out (Ramirez-Luna 1997; Montañés 2005; Bernhard 2015). Fig. 1 and Videos S1 and S2 show an aged experimental AMIL gate at École Polytechnique Fédérale de Lausanne in Switzerland (EPFL) that exhibits an oscillating behavior. This behavior was triggered by operation of the lateral offtake structures in the foreground of the photo. A wave propagating in the upstream direction can be seen. Waves, and thus oscillating behavior in general, are undesired because they are likely to affect the discharges in the main canal and the lateral offtakes.

A number of other authors have investigated instabilities related to gate operation in irrigation canals in general or more specifically instabilities of AMIL gates.

Litrico et al. (2007) developed a general method for stability analysis of automatic gates in open channels. The Saint-Venant equations (one-dimensional shallow water equations) for the open-channel dynamics were combined with a model of the automatic gate in order to derive the governing equations. The method was based on linearization and Laplace transform of these governing equations. To simplify, only a static relationship between the gate opening and the water level was assumed, i.e., the gate is in equilibrium with the water level at each instant. This was based on the assumption that gate dynamics are negligible in front of the pools dynamics. Litrico and Fromion (2009) used a similar approach also throughout.

Stability of AMIL gates was specifically investigated in Corriga et al. (1977, 1980) and Ramirez-Luna (1997). Corriga et al. (1977) investigated an AMIL gate connected to a short, level pool and considered a dynamic interaction between the gate position and the water level. A calibration of the gate that results in zero total decrement was implicitly assumed. The model was linearized and the step responses of the linear and the nonlinear systems were compared. By means of the Laplace transform, a transfer function of the linear system was derived. Instabilities were discovered and their existence was related to the value of the damping parameter.

¹Research Associate, CRYOS, Laboratory of Cryospheric Sciences, Institute of Environmental Engineering, School of Architecture, Civil and Environmental Engineering, École Polytechnique Fédérale de Lausanne, Station 2, CH-1015 Lausanne, Switzerland (corresponding author). E-mail: fabian.bernhard@alumni.epfl.ch

²Professor and Chair of Environmental Engineering, Institute for Infrastructure and Environment, School of Engineering, Univ. of Edinburgh, Edinburgh EH8 9YL, U.K. E-mail: paolo.perona@ed.ac.uk



Fig. 1. (Color) Experimental AMIL gate exhibiting oscillating behavior and creating waves

However, no study on the influence of the choice of the level pool length was done. This seems to be an important problem to address, given that the level pool is a simplifying assumption based on a model-related—not problem-related—parameter.

Corriga et al. (1980) considered two long canals connected by an AMIL gate. The Saint-Venant equations were used for the canals and the gate was modeled with an adaptation of the model developed in Corriga et al. (1977). The adaptation included the assumption of a static gate. The system was identified to be unconditionally stable for subcritical flows.

Ramirez-Luna (1997) applied the approach that was later described in Litrico et al. (2007) to three different hydromechanical gate types including AMIL gates. The findings for AMIL gates were also reported in Ramirez-Luna et al. (1998). The angular moment exerted by the water on the gate was based on Corriga et al. (1977), but it was refined by taking into account the decrement. Canal hydrodynamics were then modeled using the Saint-Venant equations. When connected to a canal, the gates were also assumed to be in a static equilibrium, based on the different time scales of the gates and canals considered in the study. Coupling of a single canal to an AMIL gate was determined to be unconditionally stable, while coupling of multiple canal reaches with AMIL gates were identified to be possibly unstable. For the latter case, a stability criterion was developed. These instabilities, however, were not attributed to the coupling of a canal reach to an AMIL gate, but rather to the interaction between canal reaches through waves.

The preceding overview shows that in most of the previous studies [apart from Corriga et al. (1977)], the gate was assumed to be in static equilibrium with the current water level. The time scale of the gate dynamics was assumed to be much shorter than the dynamics of canal reaches in typical irrigation networks. The gate dynamics

were thus neglected and the gate's purpose consisted only in determining the boundary conditions for the water level and the discharge based on the static equilibrium law (illustrated subsequently by Fig. 4).

However, observed wave formation through gate oscillation suggests that, on a local spatial scale of the order of the generated surface perturbations, the dynamics of a gate and a canal can be of similar time scales. (Wave formation was observed, for example, at an experimental gate at EPFL and is shown in Fig. 1 and Videos S1 and S2.) A dynamic gate-water level relation seems required in order to characterize the dynamics of the instability and to envision the use of such gates outside of irrigation canals, e.g., to generate nonproportional releases at water intakes (Razurel et al. 2015; Gorla and Perona 2013). In this paper, an approach similar to the one in Corriga et al. (1977) is adopted, but some basic aspects differ. The present paper uses a model that allows for a decrement [by considering an arbitrary position for the center of gravity as in Ramirez-Luna (1997)] and also distinguishes between submerged and free-flowing discharge of the gate. The gate response to perturbations depends on various gate parameters and can be investigated with a stability analysis. The influence of the level pool length l as well as the other model parameters (damping, discharge, and decrement) are investigated systematically. Lyapunov and asymptotic stability theory is used in order to determine the parameter domains in which instabilities might occur. Besides using linearized methods, a characterization of the nonlinear system is attempted.

This article can be outlined as follows. In "Technical Gate Description and Dimensionless Geometry," the technical description and the dimensionless gate parameters are presented. Then, in "Mathematical Modeling," the mathematical model describing the dynamics is derived and the relationship between the decrement and the calibration, which can be attained by altering the position of the center of gravity using the counterweights, is exposed. In "Stability Analysis and Nonlinear Effects of Control Parameters," the stability of the derived system with respect to various control parameters is assessed. In "Practical Calibration of Model Parameter \tilde{l} to Measured Dynamics," the model is calibrated to two observed dynamic behaviors of the EPFL gate.

Technical Gate Description and Dimensionless Geometry

An AMIL gate in a trapezoidal canal can be characterized by the geometrical quantities shown in Fig. 2.

Gate dimensions are described by gate axis height Y_a , gate radius R, float radius r, bottom width of gate leaf b, top width of gate leaf D, and width of float b_F .

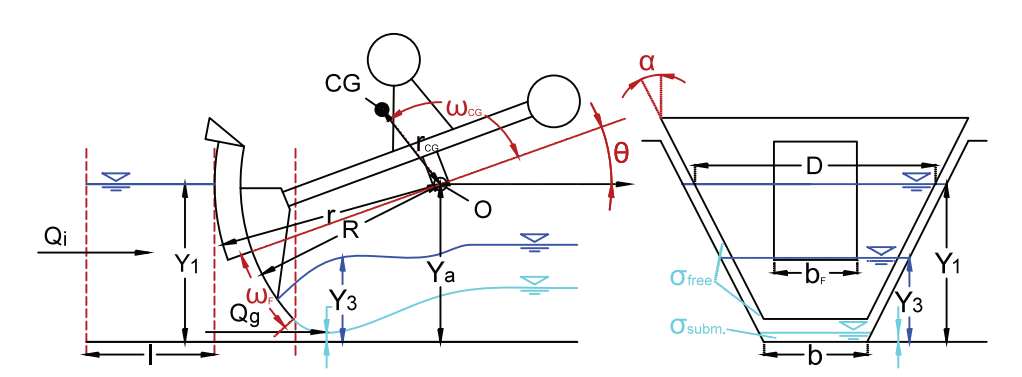


Fig. 2. (Color) Longitudinal and cross-section illustration of gate giving the geometric parameters

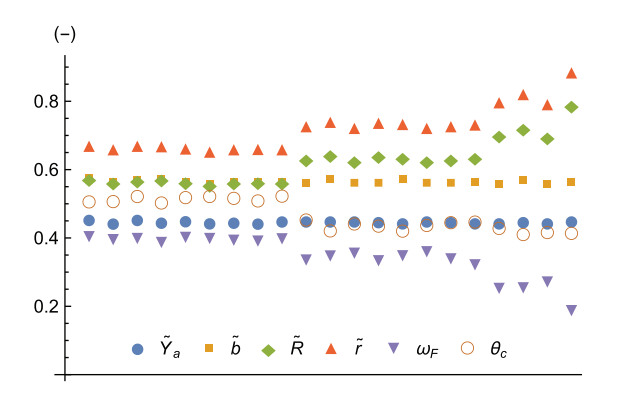


Fig. 3. (Color) Dimensionless gate parameters for 21 typical gate sizes

Table 1. Mean Values of the Dimensionless Gate Parameters for the Four Groups and the Values Used in Corriga et al. (1977)

Group	Number of gates	\tilde{Y}_a	$ ilde{b}$	$ ilde{R}$	\tilde{r}	ω_F (rad)	θ_c (rad)
1	9	0.448	0.565	0.565	0.665	0.401	0.517
2	8	0.448	0.563	0.633	0.733	0.347	0.440
3	3	0.446	0.560	0.705	0.806	0.264	0.421
4	1	0.450	0.563	0.788	0.888	0.192	0.417
Corriga et al. (1977)	1	0.430	0.567	0.633	0.658	0.314	0.434

The float is of constant width and thickness and corresponds thus to a toroid with a rectangular cross section of side lengths b_F and (r-R). The width of the float is assumed to be a fraction of the canal width at the bottom $(b_F/b = 0.8)$.

The gate position is given by θ , which is defined as the angle between the horizontal line and the lower part of the float. Other angles describe the extension of the gate leaf below float ω_F , and the position of center of gravity in polar coordinates ω_{CG} and r_{CG} . The position of the closed gate can be expressed using the preceding quantities as

$$\theta_c = \arcsin(Y_a/R) - \omega_F \tag{1}$$

The canal is characterized by the bottom width b and side slope of the trapezoidal canal wall α .

Vertical heights are defined as upstream, controlled water level Y_1 , which is the target of the regulation; downstream water level Y_3 ; and vertical opening of gate Y_g (not shown). The gate opening can be expressed as

$$Y_a = Y_a - R\sin(\theta + \omega_F) \tag{2}$$

Further quantities are needed to define the model that is developed in "Mathematical Modeling." The conservation of angular momentum refers to the angular damping coefficient c_{ω} and the moment of inertia of the movable parts of the gate about the gate axis I. Furthermore, a volume of water in front of the gate of length l is considered. Inflow and outflow of this volume are designated by Q_i and Q_g . To express the gate discharge Q_g , a discharge coefficient μ is used, combining the effect of the contraction and velocity coefficient (C_c and C_v). The slope of the canal bottom at the gate is neglected.

Brochures by gate manufacturers indicate 21 typical gate sizes with varying geometries (e.g., GEC Alsthom 1992). These 21 sizes can be grouped into four classes with distinct dimensionless

characteristics. By using the top width of the gate leaf D as scaling, dimensionless length parameters are defined as follows:

$$\tilde{Y}_a = \frac{Y_a}{D}$$
 $\tilde{b} = \frac{b}{D}$ $\tilde{R} = \frac{R}{D}$ $\tilde{r} = \frac{r}{D}$ (3)

The dimensionless gate parameters of these typical sizes are shown in Fig. 3 and the group averages are shown in Table 1. Table 1 also shows the values of the gate used in Corriga et al. (1977). To facilitate comparison, the stability investigations of the present paper are based on the same gate. The gate in Corriga et al. (1977) is based on $D=3.95~\mathrm{m},~I=4,500~\mathrm{Nms^2/rad},$ $c_\omega=20,000~\mathrm{Nms/rad},$ and $l=1~\mathrm{m}.$

Mathematical Modeling

AMIL Gate as a Dynamical System

In the following, the dynamical system description of an AMIL gate in a trapezoidal canal is derived.

Gate Movement

To determine the gate movement, Corriga et al. (1977) and Ramirez-Luna (1997) are closely followed and the moments on the gate acting about the gate axis are considered

$$I\frac{d^{2}\theta}{dt^{2}} + c_{\omega}\frac{d\theta}{dt} = M_{w}(\theta, Y_{1}) + M_{g}(\theta)$$
 (4)

 M_w and M_g = moments exerted by the water, respectively, by gravity on the gate (the sign is defined by the direction of θ , i.e., positive sign of M in the direction of closing gate). As the third moment, the effect of the angular damping coefficient c_ω is considered.

The moment by gravity M_g depends on the position of the center of gravity (ω_{CG}, r_{CG}) and the mass m of the movable parts of the gate. Referring to Fig. 2, the moment by gravity can be written as

$$M_a(\theta) = -mr_{CG}g\cos(\theta + \omega_{CG}) \tag{5}$$

To compute the moment due to the water, a hydrostatic pressure distribution along the gate leaf based on the water level Y_1 is assumed for simplification. In doing so, Corriga et al. (1977) and Ramirez-Luna (1997) are followed. Preliminary investigations (Bernhard 2015) compared the hydrostatic model to a model based on conservation of momentum over a control volume. The simpler hydrostatic model was able to reproduce more faithfully measured equilibrium positions of the EPFL gate as well as computational fluid dynamics (CFD) simulations for three different gate positions. Hence, nonhydrostatic effects are neglected. Because AMIL gates are radial gates and have a radial float with a curvature centered in the gate axis, the water pressure on the gate leaf and curved float surface does not exert a moment about the gate axis. Furthermore, it is assumed that any water mass on the downstream side of the gate does not exert any moment either. Thus, it is sufficient to consider only the bottom part of the float for the moment due to the water. The hydrostatic pressure p can be expressed as a function of θ and Y_1 and the distance \hat{r} to the gate axis

$$p(\hat{r}, \theta, Y_1) = \rho g\{Y_1 - [Y_a - \sin(\theta)\hat{r}]\} \tag{6}$$

and the moment about the gate axis can be integrated over the float bottom. This leads to the expression for the moment exerted by the water [Eq. (7)]

$$M_{w}(\theta, Y_{1}) = -b_{F} \int_{R}^{r} \hat{r} p(\hat{r}, \theta) d\hat{r}$$
 (7)

$$= -b_F \rho g \left[\frac{r^2 - R^2}{2} (Y_1 - Y_a) + \frac{r^3 - R^3}{3} \sin(\theta) \right] \tag{8}$$

The angular damping coefficient is assumed to be constant, although the elongation of the dashpot used for damping depends on the current gate position. Ramirez-Luna (1997) further treats this nonlinear effect. To include it, additional parameters describing the exact attachment configuration would need to be defined. However, when using the parameters given by Ramirez-Luna (1997), the nonlinear effect remains small ($\sim \pm 6\%$) as shown recently (Bernhard 2015) and it will therefore be neglected in this study by using a constant angular damping coefficient.

Water Level Change

Modeling a level pool allows dynamic interaction between the gate position and the water level. This level pool acts as a finite control volume for mass conservation of an incompressible fluid (Munson et al. 2009). It allows transformation of the effect of a change in the gate position via a change in discharge into a change in the water level. A level pool represents a simplification of reality and the length chosen for this reservoir is a model parameter that can be linked to reality, for example, through calibration.

Considering a length l, the level pool has a volume of

$$V = blY_1 + \tan(\alpha)lY_1^2 \tag{9}$$

Only the volume in front of the gate is considered (between the first two dashed, red lines in Fig. 2) and the volume below the gate is approximated with a constant value regardless of the gate position. Change in the level pool volume is related to the inflow and outflow by a simple reservoir volume balance equation

$$\frac{dV}{dt} = Q_i - Q_g \tag{10}$$

or in terms of water level Y_1 by using Eq. (9)

$$\frac{dY_1}{dt} = \frac{1}{l[b + 2\tan(\alpha)Y_1]}(Q_i - Q_g)$$
 (11)

Discharge through the Gate

The flow rate or discharge through the gate needs to be expressed as a function of Y_1 , θ , and Y_3 . Free and submerged flow can be distinguished depending on the downstream water depth. In case of free flow, Y_3 is replaced with C_cY_g , which represents the depth of the vena contracta.

The discharge law and coefficients used are based on Corriga et al. (1977). The law computes the total discharge as a sum of an orifice flow and free weir discharge by considering two distinct areas $\sigma_{\rm orifice}$ and $\sigma_{\rm free}$. These areas are shown for the free-flowing gate in Fig. 2 and they represent the unobstructed areas between the canal bottom and the downstream depth Y_3 ($\sigma_{\rm orifice}$) respectively between the downstream depth Y_3 and the upstream depth Y_1 ($\sigma_{\rm free}$). For simplicity, the same correction factor μ is used for both these discharges, similar to Corriga et al. (1977). To express the discharge over each area, the common assumptions of horizontal flow and atmospheric pressure within the weir nappe, as well as uniform and small approaching velocity upstream of the gate are made (Munson et al. 2009). The discharge is written as

$$Q = \int_0^{Y_1} u(\hat{y})b(\hat{y})d\hat{y} \tag{12}$$

To express the discharges for the two distinct areas with the problem parameters, the cases $Y_3 > Y_g$ (submerged) and $Y_3 < Y_g$ (e.g., free flow) need to be distinguished, where $Y_g = Y_g(\theta)$ refers to the gate opening from Eq. (2).

For $Y_3 < Y_g$ (e.g., for free flow $Y_3 = C_c Y_g$), the total discharge is decomposed in an orifice part, Q_1 ; a free weir part through the area below Y_g , Q_2 ; and a free weir part through the area on the side of the gate, Q_3 . This leads to

$$Q_q = Q_{q,\text{free}} = Q_1 + Q_2 + Q_3 \tag{13}$$

where

$$Q_1 = \mu \sqrt{2g} \{ Y_3[b + \tan(\alpha)Y_3] \} \sqrt{Y_1 - Y_3}$$
 (14a)

$$\begin{split} Q_2 &= \mu \sqrt{2g} \bigg\{ \frac{2}{3} b [(Y_1 - Y_3)^{3/2} - (Y_1 - Y_g)^{3/2}] \\ &+ \frac{4}{15} \tan(\alpha) [(3Y_3 + 2Y_1)(Y_1 - Y_3)^{3/2} \\ &- (3Y_g + 2Y_1)(Y_1 - Y_g)^{3/2}] \bigg\} \end{split} \tag{14b}$$

$$Q_3 = \mu \sqrt{2g} \left[\frac{2}{3} 2 \tan(\alpha) Y_g (Y_1 - Y_g) \right] \sqrt{Y_1 - Y_g} \qquad (14c)$$

For $Y_3 > Y_g$ (submerged case) Corriga et al. (1977) is followed by writing

$$Q_g = Q_{g,\text{submerged}} = \mu \sqrt{2g} \left(\sigma_{\text{orifice}} + \frac{2}{3} \sigma_{\text{free}} \right) \sqrt{Y_1 - Y_3}$$
 (15)

where

$$\sigma_{\rm orifice} = bY_g + Y_g^2 \tan(\alpha) + 2Y_g \tan(\alpha) (Y_3 - Y_g) \eqno(16a)$$

$$\sigma_{\text{free}} = 2Y_g \tan(\alpha)(Y_1 - Y_3) \tag{16b}$$

Corriga et al. (1977) modeled submerged conditions with a varying downstream depth, based on the discharge itself. The applied formulation does not always yield physical solutions, especially for low discharges at an almost closed gate. For submerged conditions, therefore, a fixed downstream depth, independent from the flow rate, is imposed, and the free-flowing gate is considered separately.

Next, the input discharge is normalized by introducing a hypothetical nominal discharge Q_n as a scaling

$$Q_i' = \frac{Q_i}{Q_n} \tag{17}$$

For both free and submerged gates, the nominal discharge is defined as the free discharge at completely open gate with the water level at axis height, i.e.

$$Q_n := Q_{a \text{ free}}(\theta = 0, Y_1 = Y_a, Y_3 = C_c Y_a)$$
 (18)

Combined System and Nondimensionalization

Combining the derived models for the variation of the gate position [Eq. (4)] and water level [Eq. (11)], a dynamical system governed by the following basic equations can be derived:

$$\begin{split} \frac{d^2\theta}{dt^2} &= -\frac{c_\omega}{I} \frac{d\theta}{dt} \\ &+ \frac{1}{I} \left\{ -b_F \rho g \left[\frac{r^2 - R^2}{2} (Y_1 - Y_a) + \frac{r^3 - R^3}{3} \sin(\theta) \right] \right. \\ &\left. - m r_{CG} g \cos(\theta + \omega_{CG}) \right\} \end{split} \tag{19a}$$

$$\frac{dY_1}{dt} = \frac{1}{l[b+2\tan(\alpha)Y_1]} [Q_n Q_i' - Q_g(\theta, Y_1, Y_3)]$$
 (19b)

With basic algebraic manipulations, Eq. (19) can be reformulated as

$$\frac{d^2\theta}{dt^2} = c_1 \frac{d\theta}{dt} + c_2(Y_1 - Y_a) + c_3 \cos(\theta) + c_4 \sin(\theta) \quad (\text{rad/s}^2)$$
(20a)

$$\frac{dY_1}{dt} = c_6 \frac{1}{b + 2\tan(\alpha)Y_1} [Q_n Q_i' - Q_g(\theta, Y_1, Y_3)] \quad (m/s) \quad (20b)$$

where the definitions of the constants c_1 to c_6 are reported in the Appendix.

Now the dimensionless form of the basic Eq. (20) is derived by introducing a length scale Λ and a time scale τ to scale all the lengths (e.g., Y, I, R, r) and time

$$Y = \Lambda \tilde{Y}$$
 $t = \tau \tilde{t}$

Based on the geometrical normalization it is straightforward to choose $\Lambda=D.$ A time scale $\tau=\sqrt{D/g}$ is assumed. Eq. (20) can then be reformulated as

$$\frac{d^2\theta}{d\tilde{t}^2} = C_1 \frac{d\theta}{d\tilde{t}} + C_2(\tilde{Y}_1 - \tilde{Y}_a) + C_3 \cos(\theta) + C_4 \sin(\theta) \quad (\text{rad}^2)$$
(21a)

$$\frac{d\tilde{Y}_1}{d\tilde{t}} = C_6 \frac{Q_n Q_i' - Q_g(\theta, \tilde{Y}_1, \tilde{Y}_3)}{\tilde{b} + 2\tan(\alpha)\tilde{Y}_1}$$
(21b)

where the constants C_1 to C_6 in Eq. (21) are given in the Appendix.

The system designated by Eq. (21) can be rewritten as three first-order equations

$$\frac{d}{d\tilde{t}}\theta_1 = \theta_2 \tag{22a}$$

$$\frac{d}{d\tilde{t}}\theta_2 = C_1\theta_2 + C_2(\tilde{Y}_1 - \tilde{Y}_a) + C_3\cos(\theta_1) + C_4\sin(\theta_1) \quad (22b)$$

$$\frac{d}{d\tilde{t}}\tilde{Y}_1 = \frac{C_6}{\tilde{b} + 2\tan(\alpha)\tilde{Y}_1} \{Q_n Q_i'(\tilde{t}) - Q_g[\theta_1, \tilde{Y}_1, \tilde{Y}_3(\tilde{t})]\}$$
(22c)

which is a system of the form

$$\frac{d}{d\tilde{t}}\mathbf{x} = \mathbf{F}(\mathbf{x}, \tilde{t}) \tag{23}$$

with states $\mathbf{x} = (\theta_1, \theta_2, \tilde{Y}_1)^T := (\theta, d\theta/d\tilde{t}, \tilde{Y}_1)^T$.

Eq. (22) characterizes a three-dimensional, nonautonomous, nonlinear dynamical system. The inputs to the system are $Q_i'(\tilde{t})$

and $\tilde{Y}_3(\tilde{t})$ (if submerged). By integrating system [Eq. (22)], it is possible to simulate a transient response to time dependent inputs.

However, most of the stability analysis in this study is based on the assumption that the inputs are constant in time. In that case, the inputs can be regarded as parameters of a completely autonomous system

$$\frac{d}{d\tilde{t}}\mathbf{x} = \mathbf{F}(\mathbf{x}) \tag{24}$$

Based on Eq. (24), an equilibrium point \mathbf{x}^* is defined such that $\mathbf{F}(\mathbf{x}^*) = 0$.

Calibration of the Gate and Control Parameters

In the following, it is shown how the mass of the gate and the position of the center of gravity can be related to the decrement in \tilde{Y}_1 .

The decrement is defined as the difference in the equilibrium state \tilde{Y}_1^* between a completely closed gate $\theta_1 = \theta_c$ ($Q_i' = 0$) and a completely open gate $\theta_1 = 0$. Fig. 4 shows the equilibrium states \tilde{Y}_1^* versus θ_1^* for various Q_i' .

The figure indicates the decomposition of the total decrement into a decrement above (\tilde{d}_A) and a decrement below (\tilde{d}_B) the gate axis. Given these definitions, an analytical expression for ω_{CG} and \widetilde{mr}_{CG} as a function of \tilde{d}_A and \tilde{d}_B can be derived by considering the equilibrium points at these two positions. According to the previous definition of the decrement, these gate positions are in principle $\theta_{1A}=0$ and $\theta_{1B}=\theta_c$. However, one can remain more general by using arbitrary positions $\mathbf{x}_A^*=(\theta_{1A},0,\tilde{Y}_a+\tilde{d}_A)^T$ and $\mathbf{x}_B^*=(\theta_{1B},0,\tilde{Y}_a-\tilde{d}_B)^T$. Setting Eq. (22b) at these positions to zero yields

$$\begin{cases} \widetilde{mr}_{CG} = -\frac{(\tilde{r}^2 - \tilde{R}^2)\tilde{d}_A/2 + (\tilde{r}^3 - \tilde{R}^3)\sin(\theta_{1A})/3}{\cos(\theta_{1A} + \omega_{CG})} \\ \widetilde{mr}_{CG} = -\frac{(\tilde{r}^2 - \tilde{R}^2)(-\tilde{d}_B)/2 + (\tilde{r}^3 - \tilde{R}^3)\sin(\theta_{1B})/3}{\cos(\theta_{1B} + \omega_{CG})} \end{cases}$$
(25)

Considering the specific positions $\theta_{1A} = 0$ and $\theta_{1B} = \theta_c$, Eq. (25) simplifies eventually to

$$\tan(\omega_{CG}) = \tan(\omega_{CG} + k\pi) \quad \forall \ k \in \mathbb{Z}$$

$$= \frac{1}{\tan(\theta_c)} - \frac{1}{\tilde{d}_A} \frac{2(\tilde{r}^3 - \tilde{R}^3)}{3(\tilde{r}^2 - \tilde{R}^2)} + \frac{\tilde{d}_B}{\tilde{d}_A} \frac{1}{\sin(\theta_c)}$$
(26)

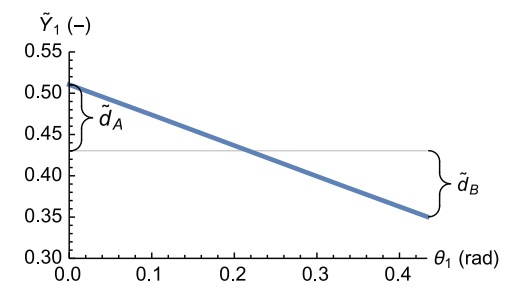


Fig. 4. (Color) Equilibrium position in the projected state space for varying Q'_i : the two components \tilde{d}_A and \tilde{d}_B (above and below gate axis) of the total decrement are shown

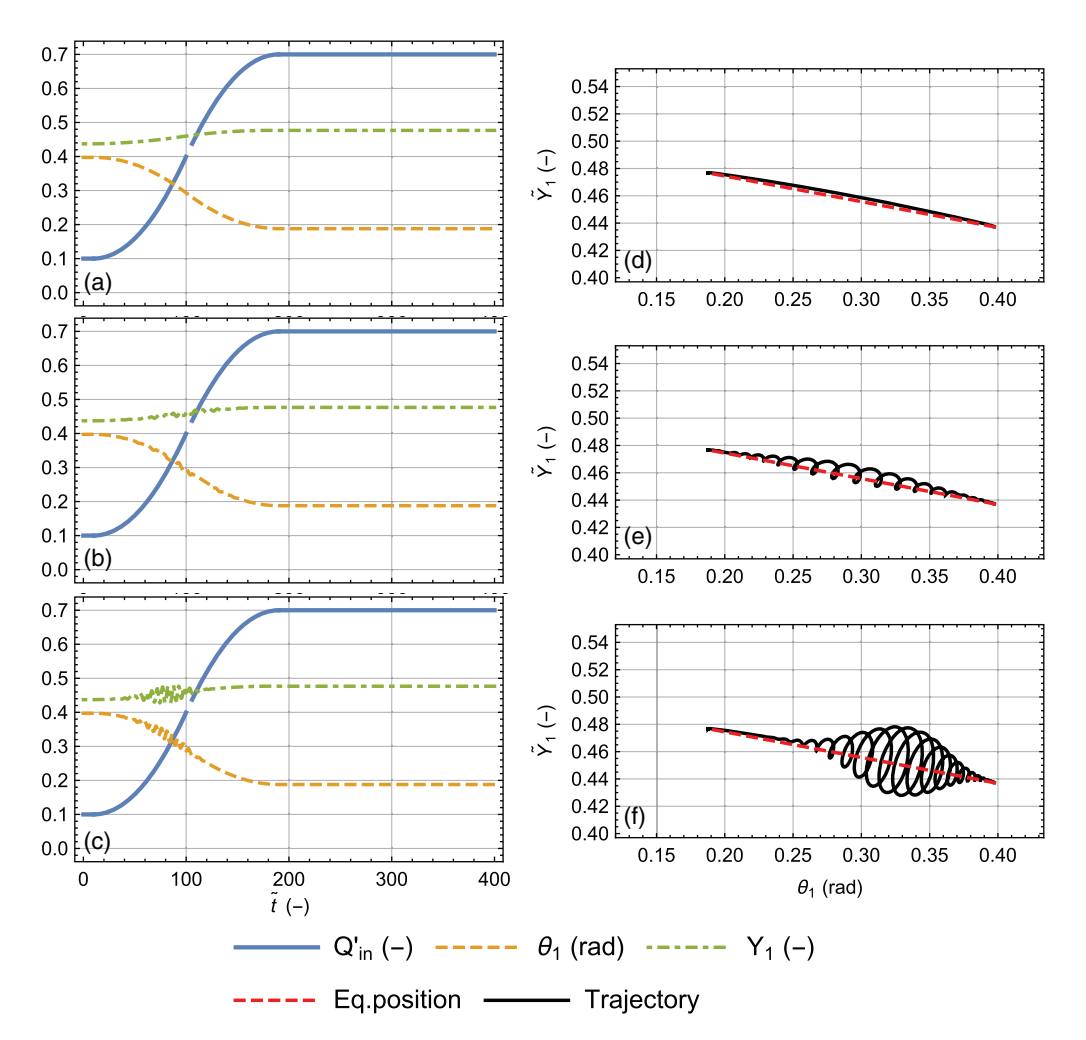


Fig. 5. (Color) (a–c) Time evolution; (d–f) projected state space trajectory of the free gate system as response to a steplike input $Q_i'(\tilde{t})$ for various damping values and level pool lengths: the red, dashed equilibrium curve is superimposed onto the state space plot; parameters $\tilde{d}_A=0.08$; (a and d) $\tilde{c}_\omega=2.25$, $\tilde{l}=0.25$; (b and e) $\tilde{c}_\omega=1.75$, $\tilde{l}=0.25$; (c and f) $\tilde{c}_\omega=2.25$, $\tilde{l}=0.1$; otherwise base parameters are from Eq. (30)

Thus, an analytical expression for ω_{CG} and \widetilde{mr}_{CG} is given by

$$\omega_{CG} = \pi + \arctan\left[\frac{1}{\tan(\theta_c)} - \frac{1}{\tilde{d}_A} \frac{2(\tilde{r}^3 - \tilde{R}^3)}{3(\tilde{r}^2 - \tilde{R}^2)} + \frac{\tilde{d}_B}{\tilde{d}_A} \frac{1}{\sin(\theta_c)}\right]$$

$$\widetilde{mr}_{CG} = \frac{1}{\cos(\omega_{CG})} \left(-\frac{\tilde{r}^2 - \tilde{R}^2}{2} \tilde{d}_A \right)$$
(27)

Note that $\tilde{d}_A \neq 0$ was assumed to derive Eq. (25). If one imposes $\tilde{d}_A = 0$, the center of gravity comes to lie perpendicular to the float bottom ($\omega_{CG} = \pi/2$) in order to have a balanced gate at complete opening $\theta_1 = 0$. Corriga et al. (1977) assumed a perfectly calibrated gate, i.e., $\tilde{d}_A = \tilde{d}_B = 0$. This corresponds to the ideal case, regulating the water level without any deviation from \tilde{Y}_a . Given $\tilde{Y}_1 = \tilde{Y}_a$, the gate is in equilibrium for any position θ_1 . Under this assumption, it follows that $\omega_{CG} = \pi/2$, and the mass has to compensate precisely the immersed float, i.e., $\widetilde{mr}_{CG} = (\tilde{r}^3 - \tilde{R}^3)/3$. Therefore, the terms C_3 and C_4 become zero and the system simplifies.

The information available in GEC Alsthom (1992) indicates a typical total decrement $\tilde{d}_A + \tilde{d}_B$ of 0.02. The following analysis assumes $\tilde{d}_B = 0$ and $\tilde{d}_A = 0.02$.

The typical functioning of the AMIL gate is illustrated by Fig. 5. A free gate, subject to a steplike increasing input $Q'_i(\tilde{t})$, is simulated starting at the equilibrium state. The simulation shown in Figs. 5(a and d) shows that with the arrival of the increased discharge the gate opens and the water level rises within the limits defined by the decrement. By opening the gate the increase in water level is mitigated. Furthermore, the behavior of the same gate can be compared with different damping coefficients and different level pool lengths [Figs. 5(b and e) and (c and f)]. While the strongly damped gate [Figs. 5(a and d)] follows the equilibrium curve closely, the less damped gate [Figs. 5(b and e)] oscillates during the transition from one equilibrium point to the other. It can be observed that the shorter level pool [Figs. 5(c and f)] influences the trajectory of these oscillations as the water level rises more quickly. The observed oscillations are possible due to the assumption of a dynamic equilibrium between gate and water level, instead of a static relationship, which would simply follow the equilibrium curve.

Once a gate geometry and size is chosen (i.e., α , \tilde{b} , \tilde{b}_F , \tilde{Y}_a , \tilde{R} , \tilde{r} , ω_F , \tilde{I}) and further constants are defined ($\mu = C_c C_v$), five control parameters ${\bf m}$ remain to completely define the autonomous system [Eq. (24)]. The function ${\bf F}$ can be recast to use these parameters ${\bf m}$ as arguments and the system becomes

$$\frac{d}{d\tilde{t}}\mathbf{x} = \mathbf{F}(\mathbf{x}, \mathbf{m}) \qquad \mathbf{m} = \begin{bmatrix} \tilde{c}_{\omega} \\ Q'_{i} \\ \tilde{d}_{A} \\ \tilde{l} \\ \tilde{Y}_{3} \end{bmatrix}$$
(28)

which is the form analyzed in the following.

Stability Analysis and Nonlinear Effects of Control Parameters

Preliminary Consideration

First, the two limit cases are investigated, in which the level pool dynamics happen on a much faster $(\tilde{l} \ll 1)$ or slower scale $(\tilde{l} \gg 1)$ than the gate dynamics. The constants C_1 , C_2 , and C_4 are of order $\mathcal{O}(1)$, C_3 is of order $\mathcal{O}(10^{-2})$, and C_6 is of order $\mathcal{O}(\tilde{l}^{-1})$.

For $\tilde{l}\gg 1$ ($C_6\to 0$) one can infer from Eq. (21) [or Eq. (20)] that oscillations of \tilde{Y}_1 are slow and \tilde{Y}_1 can be considered constant. Eq. (21a) describes the gate movement, during which a constant value for \tilde{Y}_1 can be assumed. The eigenfrequency of this subsystem is given by linearizing Eq. (21a) around an equilibrium point \mathbf{x}^* (i.e., \tilde{Y}_1^* and θ^*) which yields

$$\omega_0 = \sqrt{C_3 \sin(\theta^*) - C_4 \cos(\theta^*)} \tag{29a}$$

$$\omega = \sqrt{\omega_0^2 - \left(\frac{C_1}{2}\right)^2} = \sqrt{\omega_0^2 - \left(\frac{\tilde{c}_\omega}{2}\right)^2} \tag{29b}$$

for both the undamped (ω_0) and the damped (ω) subsystem. A critical damping $\tilde{c}_{\omega, {\rm crit}}$ separates underdamped from overdamped systems, when $\omega_0 < \tilde{c}_\omega/2$. Furthermore, when the gate is perfectly calibrated, the terms C_3 and C_4 are zero. In that case, if the water level is perturbed, Eq. (21a) does not allow a feedback of θ and is thus unstable.

For $l \ll 1$ $(C_6 \to \infty)$, the evolution of \tilde{Y}_1 becomes very fast compared with the gate. Dividing Eq. (21a) by C_6 and taking the limit of $C_6 \to \infty$ results in the static relationship $\tilde{Y}_1 = f(\theta)$, which is stable.

To summarize the findings of the limit cases, one can conclude that the system is generally stable for both small and large values of \tilde{l} . The gate and level pool subsystems are thus interfering with each other only if their time scales are similar, i.e., in an intermediate range of \tilde{l} .

In the following analysis, a base state of the control parameters $\mathbf{m_0}$ is considered. Varying one parameter at a time, the change in the qualitative behavior of the solution is observed. Equilibrium points, their stability (Lyapunov or asymptotic), one-parameter bifurcations points, and the corresponding limit cycles (including their stability) are investigated by means of a combination of analytical and numerical methods. For comparison with Corriga et al. (1977), this analysis is based on the same gate. Besides the geometric gate properties mentioned in Table 1, values are either based on Corriga et al. (1977) [$\tilde{I} = 0.0103$ and $\mu = C_c C_v = 0.65$ ($C_c = \mu/0.97$)] or stem from GEC Alsthom (1992) [$\alpha = \arctan(1/2)$]. The base set of control parameters is given by

$$\mathbf{m_0} = \begin{bmatrix} \tilde{c}_{\omega,0} \\ Q'_{i,0} \\ \tilde{d}_{A,0} \\ \tilde{l}_0 \\ \tilde{Y}_{3,0} \end{bmatrix} = \begin{bmatrix} 1.0 \\ 0.5 \\ 0.02 \\ 0.253 \\ 0.25 \end{bmatrix}$$
(30)

Influence of \tilde{c}_{ω}

Linear stability of equilibrium points for the parameters \mathbf{m}_0 can be studied with the eigenvalues of the Jacobian matrix $(\partial \mathbf{F}/\partial \mathbf{x})$ after linearization (Guckenheimer and Holmes 1993). Due to the complexity of the system, only one equilibrium point is computed numerically. The eigenvalues of the Jacobian matrix, evaluated at the equilibrium point, are shown in Fig. 6 for various values of \tilde{c}_{ω} for both free and submerged gates. In both cases, a single real and negative eigenvalue and a pair of complex conjugate eigenvalues are observed. The pair of complex eigenvalues has a positive real part for low values of \tilde{c}_{ω} , but it becomes negative above a certain limiting value. These limiting values $\tilde{c}_{\omega, \mathrm{lim}}$ are 1.670 and 1.097 for the free and the submerged gate, respectively. The equilibrium point is thus unstable at the lower values, but is stabilized at the higher damping. Numerical simulations with the nonlinear system [Eq. (28)] using slightly perturbed initial conditions confirmed this stabilizing value of \tilde{c}_{ω} . The eigenvalues remain in the left halfplane, i.e., stable, for further increases in the damping parameter \tilde{c}_{ω} . Above another specific value of \tilde{c}_{ω} , the pair of complex conjugate eigenvalues becomes real valued ($\tilde{c}_{\omega, \rm crit} = 42.0$ and 14.8, respectively). This critical damping value illustrates the effect of the level pool [Eq. (21b)], which was neglected for $\tilde{c}_{\omega,\text{crit}}$ in the preliminary considerations. The qualitative characteristics of this plot of the eigenvalues in Fig. 6 are similar to the plot of the roots of the transfer function shown in Corriga et al. (1977).

Simultaneous passing of the imaginary axis by two eigenvalues, while no other eigenvalue has zero real part, indicates a Hopf bifurcation at the parameter value of the crossing (Guckenheimer and Holmes 1993). A Hopf bifurcation describes the emergence of limit cycles from an equilibrium point when a parameter is varied (Guckenheimer and Holmes 1993; Ermentrout 2002).

The observed bifurcation of the nonlinear system at $\tilde{c}_{\omega, \text{lim}}$ is investigated with the software package *XPPAUT* (Ermentrout 2002), containing the numerical continuation software *AUTO*. Fig. 7 shows the one-parameter bifurcation diagrams for various control parameters for the submerged system. These diagrams show the gate position θ_1 in equilibrium position for the minimum and maximum values on the limit cycles, as well as the periods \tilde{T} of the limit cycles. Stable limit cycles emerge when the damping is below the limiting value. Having stable limit cycles, the system undergoes a supercritical Hopf bifurcation.

The existence of these periodic solutions is confirmed numerically. Periodic solutions, found using a boundary value approach, are shown in Fig. 8. [The applied procedure is based on Higgins (2013), which also explains the derivation of the boundary value problem.]

The evolution of the gate position and water level during a cycle and the trajectory in the state space are shown for the free gate [Fig. 8(a)] and the submerged gate [Fig. 8(b)] for $\mathbf{m_0}$. Both systems are shown for the same damping ratios $\tilde{c}_{\omega}/\tilde{c}_{\omega,\text{lim}}$, and Q_i' is chosen for each system separately to yield similar equilibrium positions in θ_1 . The trajectories are in agreement with the values shown by Fig. 7. A phase shift in the trajectories between gate position θ_1 and water level \tilde{Y}_1 can be observed. The periods and Floquet multipliers of these periodic solutions are shown in Table 2. With only one Floquet multiplier of magnitude 1 or higher, the limit cycles are stable.

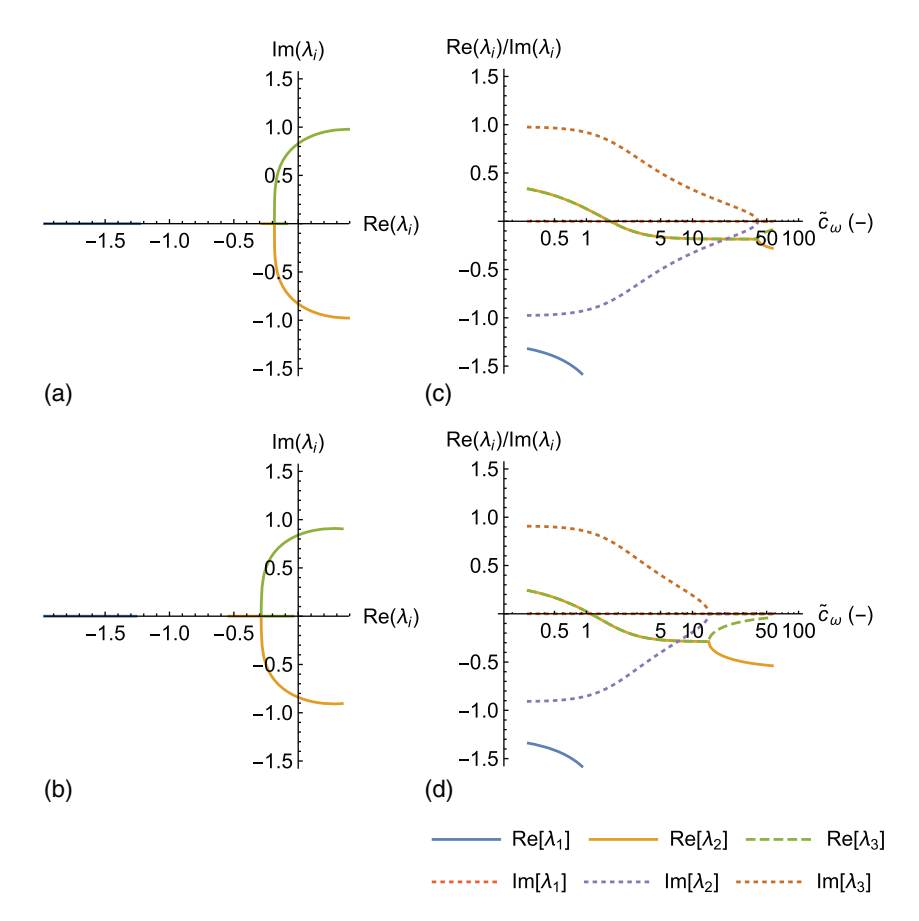


Fig. 6. (Color) Eigenvalues of the (a and c) free; (b and d) submerged autonomous gate system for base parameters $\mathbf{m_0}$ and varying \tilde{c}_{ω} : (a and b) complex plane; (c and d) real and imaginary components

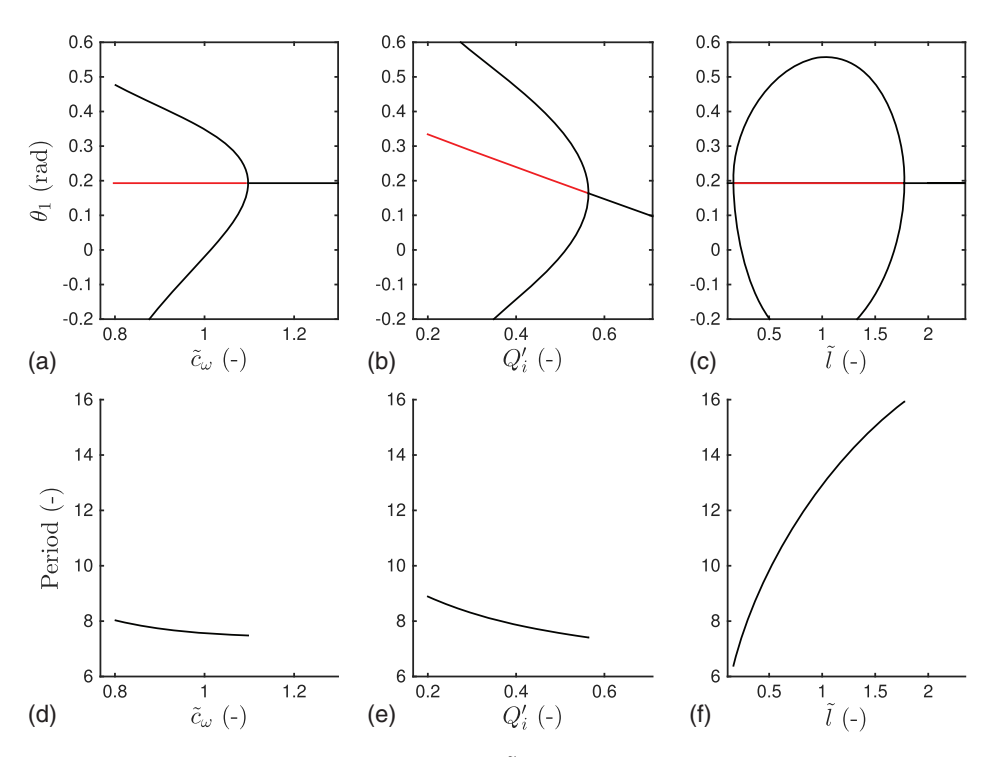


Fig. 7. (Color) One-parameter bifurcations for the control parameters \tilde{c}_{ω} , \tilde{l} , and Q'_i , based on the submerged gate with $\mathbf{m_0}$: the diagrams show the minimum and maximum value during a limit cycle and the equilibrium point in θ_1 and the periods of the limit cycles; red indicates an unstable, black a stable equilibrium point and limit cycle; zoom-in on the \tilde{c}_{ω} -values used in Fig. 8 is provided in Fig. S1

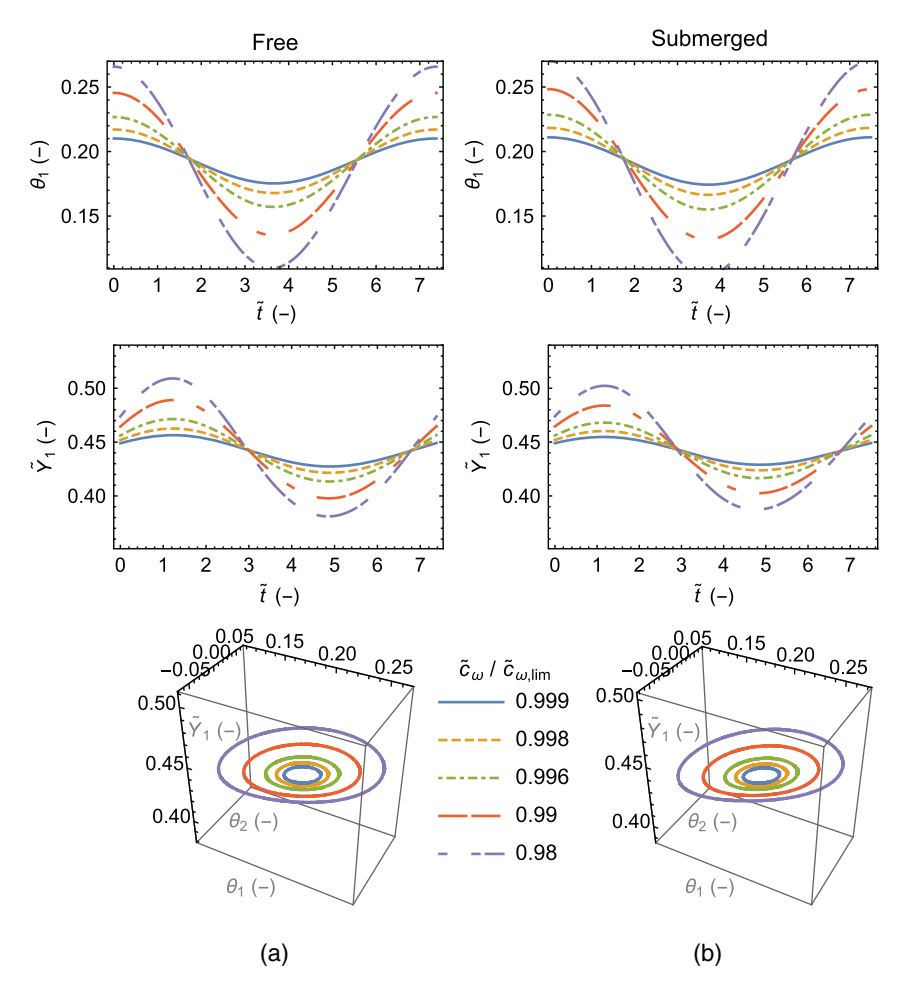


Fig. 8. (Color) Time evolution of the gate position and water level during a limit cycle and the trajectory in the state space are shown for the (a) free gate; (b) submerged gate for various damping ratios. $Q'_i = 0.64$ (free) or $Q'_i = 0.5$ (submerged), otherwise $\mathbf{m_0}$

Table 2. Periods and Floquet Multipliers for the Different Periodic Solutions Shown in Fig. 8

c_{ω}								
$\tilde{c}_{\omega, \mathrm{lim}}$	Period	Floquet 1	Floquet 2	Floquet 3				
	Free gate							
0.999	28.847	1.000	0.996	2.877×10^{-7}				
0.998	28.848	1.000	0.992	2.902×10^{-7}				
0.996	28.850	1.000	0.985	2.955×10^{-7}				
0.990	28.857	1.000	0.962	3.119×10^{-7}				
0.980	28.869	1.000	0.923	3.409×10^{-7}				
		Submerged gate						
0.999	29.491	1.000	0.996	1.537×10^{-6}				
0.998	29.491	1.000	0.992	1.544×10^{-6}				
0.996	29.492	1.000	0.984	1.559×10^{-6}				
0.990	29.495	1.000	0.961	1.603×10^{-6}				
0.980	29.502	1.000	0.922	1.676×10^{-6}				

Influence of Q'

As a first assessment of the influence of the parameter Q_i' , the linear stability of the equilibrium point for the base parameters $\mathbf{m_0}$ is considered. The eigenvalues of the Jacobian matrix are shown in Fig. 9 for various values of Q_i' for the submerged gate. The free gate is not shown, behaving qualitatively similarly. Because the equilibrium point depends on the value of Q_i' , the Jacobian matrix needs to be reevaluated at each (numerically found) equilibrium point.

Again, there exists a limiting value $Q'_{i,\text{lim}}$ of 0.5638 (0.8217 for the free gate) stabilizing the system. Again, numerical simulations with perturbed initial conditions confirmed these limiting values.

The evolution of the eigenvalues in the complex plane for varying Q_i' is similar to the evolution for varying \tilde{c}_{ω} . A supercritical Hopf bifurcation for the parameter Q_i' is expected and confirmed by Fig. 7(b).

The resulting periodic solutions for values below $Q'_{i,\text{lim}}$ are qualitatively similar to the ones shown in Fig. 8 for variations in \tilde{c}_{ω} . The magnitude of the oscillations increases with decreasing Q'_i , an observation that can readily be inferred from the bifurcation diagram.

The response to the steplike input $Q_i'(t)$ shown in Fig. 5 illustrates the change in stability due to Q_i' . Fig. 10 compares the response to such a steplike input for the free and submerged gate using the same damping ratio $\tilde{c}_{\omega}/\tilde{c}_{\omega, \text{lim}} = 0.61$, based on $\tilde{c}_{\omega, \text{lim}}$ for the initial value of Q_i' . The input $Q_i'(\tilde{t})$ increases from 0.2 to 0.7. Both gates are unstable at the initial value of Q_i' and start to oscillate. The systems stabilize with increasing discharge because they are stable at the final value of Q_i' . The damping \tilde{c}_{ω} of the submerged gate used for the simulation is lower than the one of the free gate (1.80 versus 1.17).

Influence of \tilde{d}_A and \tilde{Y}_3

The relationship between Q'_i and $\tilde{c}_{\omega, \text{lim}}$ is illustrated by Fig. 11. It shows the free gate system using various values for \tilde{d}_A in

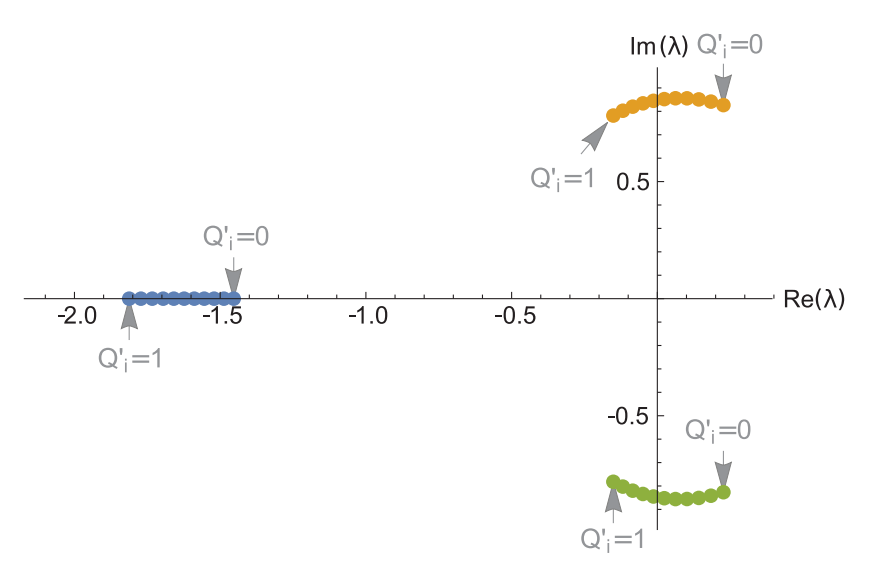


Fig. 9. (Color) Eigenvalues of the submerged gate system for base parameters \mathbf{m}_0 and varying Q_i'

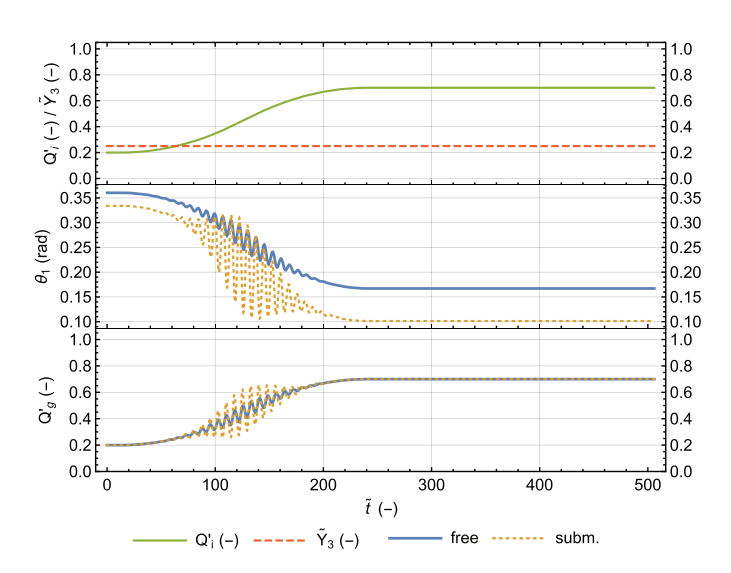


Fig. 10. (Color) Response in θ_1 and Q_g' (= Q_g/Q_n) of the free (blue, solid) and submerged (yellow, dashed) gate to a steplike increase in Q_i' (green, solid): besides $Q_i'(\tilde{t})$ (indicated), $\tilde{c}_{\omega}/\tilde{c}_{\omega,\text{lim}} = 0.61$ and $\mathbf{m_0}$

Figs. 11(a and c), while the submerged gate system uses $d_{A,0} = 0.02$, but various submergence depths \tilde{Y}_3 in Figs. 11(b and d). Generally, the limiting values $\tilde{c}_{\omega,\text{lim}}$ decrease with increasing discharge (i.e., larger gate openings), illustrating again the stabilizing effect of large Q_i' . A shift in the x-axis can be observed between the plots showing the limiting values for the same system, but either using Q_i' or θ_{eq} [Figs. 11(b and d)]. These shifts depend on the value of \tilde{d}_A or \tilde{Y}_3 . This is caused by the influence of these parameters on the equilibrium position θ_{eq} for the same Q_i' .

An increase in the decrement \tilde{d}_A might have a stabilizing or destabilizing effect on the system, i.e., requiring a lower or higher damping, depending on the Q_i' considered. However, the destabilizing effect seems to be explained through the change in the equilibrium position $\theta_{\rm eq}$ for different decrements. Indeed, judging only by the free gate plot against $\theta_{\rm eq}$ in Fig. 11(c), an increase in the decrement decreases the $\tilde{c}_{\omega, \rm lim}$ for almost all equilibrium positions.

For the submerged gate, an increase in the downstream depth \tilde{Y}_3 stabilizes the gate. It is likely that this is caused by the reduced sensitivity of the gate discharge Q_g to the gate position θ_1 (i.e., a smaller $\partial Q_g/\partial \theta$). This can be observed for the various values of \tilde{Y}_3 in Figs. 11(b and d).

Influence of Î

Already highlighted by the preliminary considerations, the system is generally stable in the limits $\tilde{l} \ll 1$ and $\tilde{l} \gg 1$, unless the total decrement is set to zero, where stability occurs only in the lower limit $\tilde{l} \ll 1$. These observations are confirmed by Fig. 12, showing the real part of the second eigenvalue of the linearized system as a function of \tilde{l} . The bifurcation diagram for \tilde{l} in Fig. 7 identifies two supercritical bifurcations. The period of the limit cycle, shown in the same figure, differs strongly.

Fig. 13 shows the identified limiting damping parameter $\tilde{c}_{\omega, \mathrm{lim}}$ as a function of \tilde{l} . It can be observed that the value of \tilde{l} resulting in the highest $\tilde{c}_{\omega, \mathrm{lim}}$ depends on the value of \tilde{d}_A .

Practical Calibration of Model Parameter \tilde{I} to Measured Dynamics

The level surface is a simplifying assumption, using a model-related—not problem-related—parameter \tilde{l} . In the following, this parameter \tilde{l} is calibrated to observed wave interactions with a canal. Video measurements were performed of the dynamical behavior of the experimental gate at EPFL. Two distinct dynamic regimes have been recorded. Videos S1 and S2 show the two behaviors. The gate position during the two dynamic responses is shown in Fig. 14.

In Behavior A, the upper end of the canal reach upstream of the gate, situated at a distance L, acts as a reflecting boundary for incoming waves. A periodic solution develops as the waves in the canal and the gate synchronize. The periodic solution corresponds to a standing wave in the canal with the gate oscillating at the same frequency.

Behavior B corresponds to a transient response, describing the gate rising after being initially locked in the closed position. Over the short period of time considered, the reflecting upstream

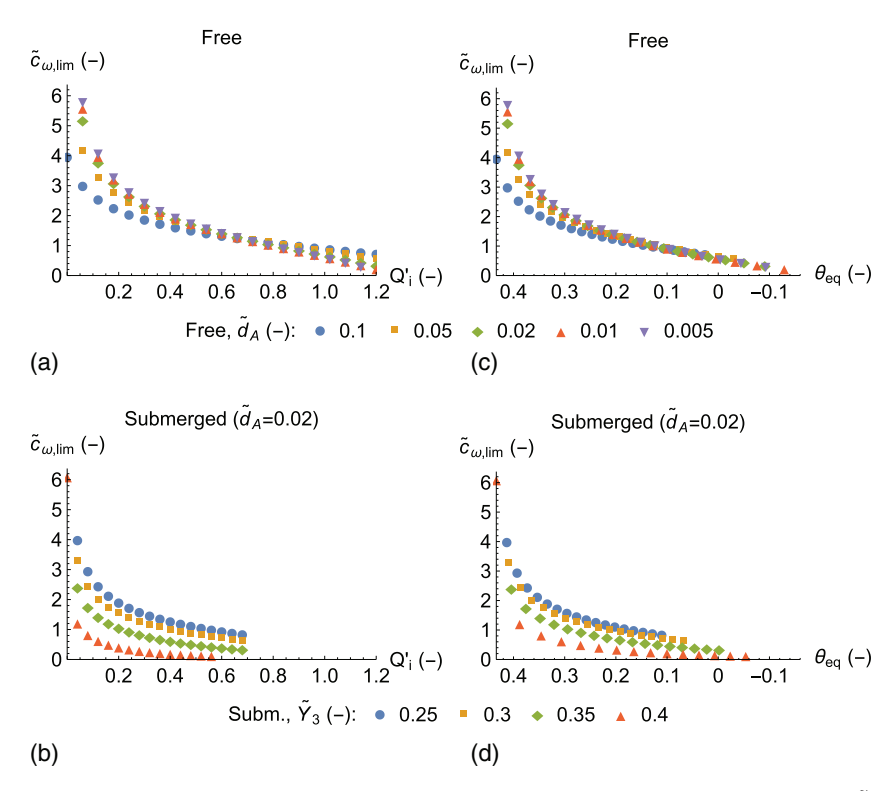


Fig. 11. (Color) Limiting damping $\tilde{c}_{\omega, \text{lim}}$ as a function of Q_i' for the (a and c) free gate system with various values for \tilde{d}_A and the (b and d) submerged gate system with $\tilde{d}_{A,0} = 0.02$ and various submergence depths \tilde{Y}_3

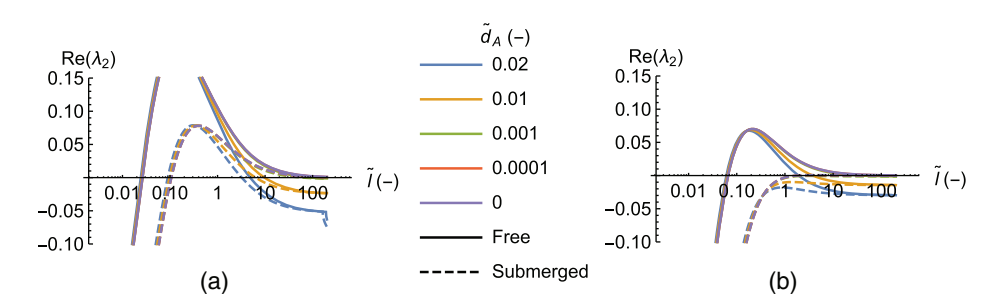


Fig. 12. (Color) Real part of second eigenvalue of linearized systems as a function of level pool length l and for various decrements \tilde{d}_A : (a) standard damping $\tilde{c}_{\omega} = \tilde{c}_{\omega,0} = 1.0$; (b) stronger damping of $\tilde{c}_{\omega} = 1.3$

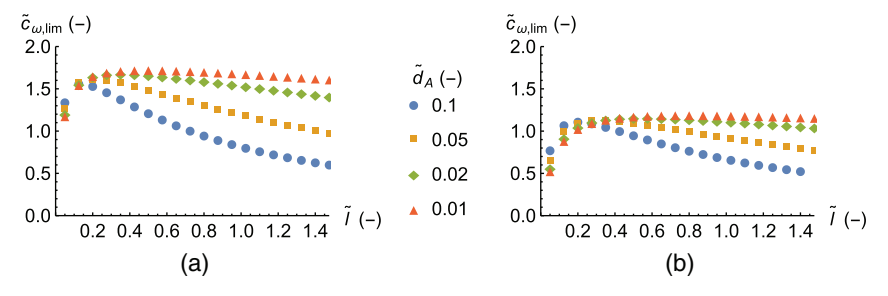


Fig. 13. (Color) Limiting damping $\tilde{c}_{\omega, \text{lim}}$ as a function of \tilde{l} for the (a) free; (b) submerged gate system with various values for \tilde{d}_A otherwise \mathbf{m}_0

boundary has no effect on the gate because the perturbations generated by the gate travel with a finite speed.

Both measurements were taken under free-flowing conditions. The gate setup at EPFL is described by the following measured

quantities: D = 0.81, R = 0.63, r = 0.685, $Y_a = 0.367$, b = 0.46, $b_F = 0.36$ m, $\omega_F = 0.173$ m/R, $\alpha = \arctan(1/2)$, $\omega_{CG} = 1.61$ rad, and $mr_{CG} = 8.13$ kg m; and the following estimated dynamic properties: I = 7.67 Nms²/rad and $c_{\omega} = 69.0$ Nms/rad.

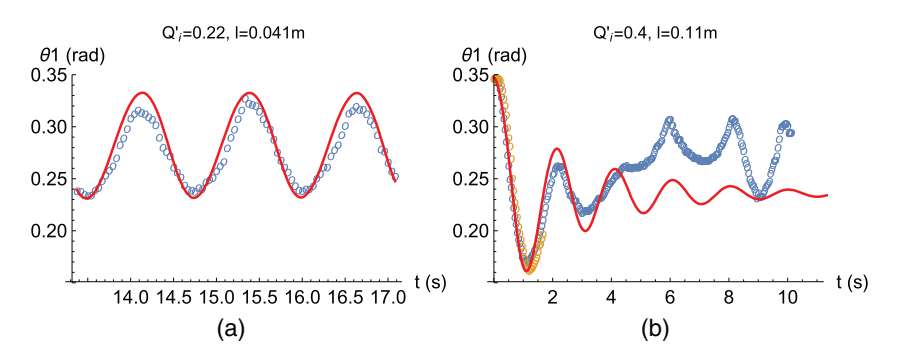


Fig. 14. (Color) Measurements (circles) and model simulations (lines) of the two dynamic behaviors measured on the EPFL gate: (a) three cycles of the oscillating gate when the standing waves have formed; (b) rising of the gate (blue and orange circles correspond to two measurements of the phenomenon)

The canal reach ends at a distance L=4.17 m upstream of the gate leaf in a boundary, where the inflow enters the canal reach through the bottom part.

The length of the level pool volume can be calibrated to reproduce the observed behavior. While Behavior A is representative of a short canal reach under the influence of an upstream reflecting boundary, Behavior B can describe an infinitely long canal reach, where the generated perturbations are not reflected upstream. These two situations can be characterized by two different values of \tilde{l} .

For Behavior A, the standing wave in the canal can be described with standing wave theory (SWT). The sensitivity of the frequency of the gate to the model parameter \tilde{l} can be observed in the bifurcation diagram (Fig. 7). This allows estimation of \tilde{l} for a given frequency. Both of these approaches can be combined to estimate the parameter \tilde{l} for AMIL gates with canals of various lengths L showing standing wave behavior.

In the observed case, the ratio of the flow velocity to the wave celerity is small $(U_0/c \ll 1)$. Therefore, classic SWT using a constant celerity in both directions is applied. Standing wave theory allows determination of the frequency of a specific mode for a canal of a given length L. Based on that the parameter, l can be determined by adjusting the frequency of the gate to the standing wave in the canal. In Behavior A, both ends of the canal were antinodes, i.e., the amplitude of the oscillations is at its maximum. This can be translated to boundary conditions prescribing the gradient of the water level to be zero. The frequency of the modes is then given by $f_n = nc/(2L)$, where the wave celerity is related to the equilibrium water level by $c = \sqrt{gY_1^*}$. The observed Behavior A corresponds to the mode with n = 4, resulting in a theoretical frequency by wave theory of $f_{4,\text{SWT}} = 0.93 \text{ Hz}$ or $\omega_{4,\text{SWT}} =$ 5.85 rad/s (using $Y_1^* = 0.385$ m for both). The level pool length required to obtain the same frequency of gate oscillations is $l_{SWT} = 0.043$.

However, the frequency of the observed behavior does not exactly coincide with the one predicted by standing wave theory. Further studies including nonlinear effects may explain such differences. The measured frequency was $f_{\rm meas}=0.81$ Hz or $\omega_{\rm meas}=5.09$ rad/s. The level pool length corresponding to this frequency is $\tilde{l}_{\rm meas,A}=0.05$.

Behavior B is considered over roughly two oscillation cycles, corresponding to the time before the perturbations return. (The inflow Q_i was adapted to compensate the flow above the gate that occurred during the measurement.) A parameter $\tilde{l}_{\text{meas,B}} = 0.14$ was calibrated for this behavior. Transient effects from the reflection of the waves remain after the two oscillations cycles, but eventually the gate stabilizes.

The model simulation for the parameters $\tilde{l}_{\text{meas},A}$ and $\tilde{l}_{\text{meas},B}$ and two different inflow discharges are superimposed onto Fig. 14. Using the value of $\tilde{l}=0.253$ from Corriga et al. (1977) would result in too low frequencies to reproduce either Behavior A or B.

In conclusion, the choice of \tilde{l} thus depends on the type of dynamic one wants to reproduce.

Conclusion and Outlook

In this article, a mathematical model was developed based on Corriga et al. (1977) and Ramirez-Luna (1997) and investigated with respect to various control parameters. The model was used to reproduce two kinds of dynamic behavior of an experimental gate. For the calibration of the counterweights, an analytical formula permitting the imposition of a specified decrement was presented. The stability analysis allowed determination of limiting values for the damping parameter $\tilde{c}_{\omega,\text{lim}}$. A change in behavior at these limiting values from stable equilibria to stable periodic solutions—a supercritical Hopf bifurcation—was shown. The periodic solutions are not desired in irrigation canals, leading to fluctuations of discharges in the main canal and lateral offtakes. The constant inflow parameter Q_i' exhibits similar influence on the system as $\tilde{c}_{\omega,\text{lim}}$.

The identified limiting values depend on the model parameter \tilde{l} . It is therefore important to use a representative level pool length \tilde{l} or to simply select the most conservative damping $\tilde{c}_{\omega, \text{lim}}$ among the estimates obtained with a wide range of \tilde{l} .

In view of the typically slow canal dynamics in irrigation canal networks (Corriga et al. 1980; Ramirez-Luna 1997), the dynamic interactions between the water level and the gate are considered negligible by other authors and the simplification of a static gate appropriate. On the other hand, the model based on a level pool, used throughout this work, allows consideration of the dynamic interaction between the local water level and the AMIL gate. This dynamic interplay might become more important under circumstances where faster water level dynamics are present (e.g., irrigation canals exhibiting resonance behavior or situations outside of irrigation canals). Refraining from the static gate simplification, by using the level pool model, seems more appropriate in those circumstances.

To complement existing studies (e.g., Ramirez-Luna 1997), the model developed here can suggest a different approach to study interaction of AMIL gates installed in series. In canals exhibiting strong resonance behavior and weak wave attenuation, waves generated by a nonstatic gate—water level relationship might reach and influence other AMIL gates upstream or downstream.

To operate run-of-the-river hydropower plants, nonproportional water distribution from rivers is an efficient alternative to fixed-percentage (proportional) releases of the incoming flow

(Razurel et al. 2015; Gorla and Perona 2013; Perona et al. 2013). AMIL gates might constitute a possible energy-free means for this repartitioning. The authors envision that the combination of a weir in the river and an AMIL gate with an adapted float form in the derived canal might allow implementation of nonproportional dynamic environmental flows, hence the importance of studies that address stability conditions.

Appendix. Constants

Constants for a dimensional system:

$$c_1 = -\frac{c_\omega}{I} \quad (s^{-1}) \tag{31a}$$

$$c_2 = -\frac{b_F \rho g}{I} \frac{r^2 - R^2}{2} \quad [\text{rad}/(\text{s}^2 \,\text{m})]$$
 (31b)

$$c_3 = -\frac{b_F \rho g}{I} \frac{m r_{CG}}{b_F \rho} \cos(\omega_{CG}) \quad (\text{rad/s}^2)$$
 (31c)

$$c_4 = -\frac{b_F \rho g}{I} \left[\frac{r^3 - R^3}{3} - \frac{m r_{CG}}{b_F \rho} \sin(\omega_{CG}) \right] \quad (\text{rad/s}^2) \qquad (31d)$$

$$c_6 = \frac{1}{l} \quad (\mathbf{m}^{-1}) \tag{31e}$$

Constants for a dimensionless system:

$$C_1 = c_1 \tau = \tilde{c}_\omega = \frac{c_\omega}{I} \sqrt{\frac{\Lambda}{g}}$$
 (32a)

$$C_2 = c_2 \tau^2 \Lambda = -\frac{1}{\tilde{I}} \frac{\tilde{r}^2 - \tilde{R}^2}{2}$$
 (rad) (32b)

$$C_3 = c_3 \tau^2 = -\frac{1}{\tilde{I}} \widetilde{mr}_{CG} \cos(\omega_{CG}) \quad \text{(rad)}$$
 (32c)

$$C_4 = c_4 \tau^2 = -\frac{1}{\tilde{I}} \left[\frac{\tilde{r}^3 - \tilde{R}^3}{3} - \widetilde{m} r_{CG} \sin(\omega_{CG}) \right] \quad (\text{rad}) \quad (32d)$$

$$C_6 = \frac{\tau}{\Lambda} \frac{c_6}{\Lambda} = \frac{1}{\sqrt{g} \Lambda^{5/2}} \frac{1}{\tilde{l}} \quad (\text{s/m}^3) \tag{32e}$$

$$\tilde{c}_{\omega} = \frac{c_{\omega}}{I} \sqrt{\frac{\Lambda}{q}} \tag{33a}$$

$$\tilde{I} = \frac{I}{\rho \tilde{b}_F \Lambda^5} \quad (\text{rad}^{-1}) \tag{33b}$$

$$\widetilde{mr}_{CG} = \frac{mr_{CG}}{\widetilde{b}_F \rho \Lambda^4} \tag{33c}$$

Acknowledgments

The Swiss National Science Foundation is greatly acknowledged for funding the projects REMEDY (Grant No. PP00P2153028/684 1). The Swiss Commission for Technology and Innovation

(CTI) is greatly acknowledged for funding the Swiss Competence Center for Energy Research—Supply of Electricity (SCCER-SoE). Paolo Perona wishes to thank the Climatology Research Group at the Institute of Geography of the University of Bern for hosting him as academic guest.

Supplemental Data

Fig. S1 and Videos S1 and S2 with the corresponding Data S1 and S2 are available online in the ASCE Library (www.ascelibrary.org).

References

AUTO-07p [Computer software]. Concordia Univ., Montreal.

Bernhard, F. (2015). "Dynamical behavior of automatic gates for upstream water surface regulation in irrigation canals." Master thesis, École polytechnique fédérale de Lausanne (EPFL), Lausanne, Switzerland.

Cassan, L., Baume, J.-P., Belaud, G., Litrico, X., Malaterre, P.-O., and Ribot-Bruno, J. (2011). "Hydraulic modeling of a mixed water level control hydromechanical gate." *J. Irrig. Drain. Eng.*, 10.1061 /(ASCE)IR.1943-4774.0000305, 446–453.

Corriga, G., Patta, F., Tola, S., and Usai, G. (1977). "La dinamica delle paratoie autolivellanti nelle reti di distribuzione a pelo libero [reti di irrigazione]." *Idrotecnica*, 6, 249–255.

Corriga, G., Sanna, S., and Usai, G. (1980). "Frequency response and dynamic behaviour of canal networks with self-levelling gates." Appl. Math. Modell., 4(2), 125–129.

Ermentrout, B (2002). Simulating, analyzing, and animating dynamical systems, Society for Industrial and Applied Mathematics, Philadelphia.

GEC Alsthom. (1992). "Amil gates—Constant upstream level control in reservoirs and canals." (http://www.canari.free.fr/papers/neyrpic_amil_fr.pdf) (Nov. 14, 2015).

Gorla, L., and Perona, P. (2013). "On quantifying ecologically sustainable flow releases in a diverted river reach." J. Hydrol., 489, 98–107.

Guckenheimer, J., and Holmes, P. (1993). Nonlinear oscillations, dynamical systems, and bifurcations of vector fields, Springer, New York.

Higgins, B. G. (2013). "Stability analysis of periodic solutions." (https://sites.google.com/site/chemengwithmathematica/home/numerical-methods) (Nov. 14, 2015).

Litrico, X., Belaud, G., and Fromion, V. (2007). "Stability analysis of automatic water level control gates in open-channels." 46th IEEE Conf. on Decision and Control, 2007, IEEE, New York, 1591–1596.

Litrico, X., and Fromion, V. (2009). *Modeling and control of hydrosystems*, Springer, London.

Montañés, J. L. (2005). Hydraulic canals: Design, construction, regulation and maintenance, Taylor & Francis, London.

Munson, B. R., Young, D. F., Okiishi, T. H., and Huebsch, W. W. (2009). Fundamentals of fluid mechanics, Wiley, New York.

Perona, P., Dürrenmatt, D. J., and Characklis, G. W. (2013). "Obtaining natural-like flow releases in diverted river reaches from simple riparian benefit economic models." *J. Environ. Manage.*, 118, 161–169.

Ramirez-Luna, J. (1997). "Modélisation des ouvrages frontaux et latéraux dans les canaux d'irrigation." Ph.D. thesis, Ecole Nationale du Génie Rural, des Eaux et des Fôrets (ENGREF), Ecole Nationale du Génie Rural, des Eaux et des Fôrets (ENGREF), Paris.

Ramirez-Luna, J., Baume, J., De León-Mojarro, B., Ruiz-Carmona, V., and Sau, J. (1998). "Wave motion stability for coupled canal pool-amil gate systems." 1998 IEEE Int. Conf. on Systems, Man, and Cybernetics, Vol. 4, IEEE, San Diego, 3868–3873.

Razurel, P., Gorla, L., Crouzy, B., and Perona, P. (2015). "Non-proportional repartition rules optimize environmental flows and energy production." *Water Resour. Manage.*, 30(1), 1–17.

Rogers, D. C., and Goussard, J. (1998). "Canal control algorithms currently in use." *J. Irrig. Drain. Eng.*, 10.1061/(ASCE)0733-9437(1998)124: 1(11), 11–15.